

Intermittency of passive-scalar decay: strange eigenmodes in random shear flows

J. Vanneste*

School of Mathematics

University of Edinburgh, UK

May 16, 2006

*Author address: J. Vanneste, School of Mathematics, University of Edinburgh, King's Buildings, Edinburgh EH9 3JZ, UK. email: J.Vanneste@ed.ac.uk

The decay of the concentration of a passive scalar released in a periodic shear flow with random time dependence is examined. Periodic boundary conditions are assumed, placing the problem in the strange-eigenmode regime where the concentration decay is exponential in the long-time limit. The focus is on the limit of small diffusivity $\kappa \ll 1$ (large Péclet number) which is studied using a combination of asymptotic methods and numerical simulations. Two specific flows are considered: both have a sinusoidal velocity profile, but the random function of time is either (i) the amplitude of the sinusoid or (ii) its phase. The behaviour of the passive scalar in each flow is very different. The decay rate (or Lyapunov exponent) λ , in particular, which characterises the long-time decay in almost all flow realisations, scales like $\kappa^{2/3}$ in (i) and $\kappa^{3/8}$ in (ii).

The temporal intermittency of the scalar decay, associated with fluctuations in the speed of decay, is examined in detail. It is quantified by comparing the decay rate λ with the decay rates γ_p of the ensemble-averaged p -th moment of the concentration. The two flows exhibit some intermittency, with $\gamma_p \neq p\lambda$. It is however much weaker for flow (i) where the γ_p and λ satisfy $\kappa^{2/3}$ power laws, than for flow (ii) where the γ_p are proportional to $\kappa^{1/2}$ and therefore asymptotically smaller than λ . The results for flow (ii) highlight the possible difficulty in relating the behaviour of the passive scalar in single flow realisations to predictions made for ensemble-averaged quantities such as concentration moments.

1 Introduction

The aim of this paper is to examine the temporal intermittency that can arise when a passive scalar decays through advection and diffusion in a flow with complex time dependence. For smooth flows in bounded domains, it has been recognised since the work of Pierrehumbert [1] that the passive-scalar decay is exponential in the long-time limit. This is obvious for time-independent or time-periodic flows — the decay rate is then an eigenvalue or a Floquet exponent [2] — but less so for flows that are stationary random functions of time. In this case, one needs to invoke the ergodic multiplicative theory [3, 4] to argue that the decay rate is (the negative of) the largest Lyapunov exponent associated with the advection–diffusion equation. The spatial structure of the decaying scalar, termed ‘strange eigenmode’

by Pierrehumbert [1], is associated with the corresponding (random) invariant subspace [3].

The issue of temporal intermittency arises when the finite-time behaviour of the decaying scalar is considered. A strongly intermittent decay is characterised by large transient variations in the rate at which the scalar concentration decreases: for some time this decrease can be much faster or much slower than that predicted by the decay rate. Over long time scales, of course, the periods of anomalously fast and slow decay average out to lead to the infinite-time decay rate. Strong intermittency also implies that there is a large variability in the scalar decay between different realisations of the flow. This is to be contrasted with the behaviour in weakly intermittent systems: in these, the decay for even small observation periods is systematically well predicted from the decay rate, and each realisation of the flow is roughly identical. The difference is clearly important in practice, since it is often necessary to predict the behaviour of single realisations of a flow.

To quantify temporal intermittency, it is natural to define finite-time decay rates, in analogy with the finite-time Lyapunov exponents used for finite-dimensional dynamical systems [5]. Unlike the (infinite-time) decay rate, λ say, which is deterministic and relevant to almost all flow realisations, the finite-time decay rates λ_t are random variables. Their statistical distribution and the manner with which this distribution collapses to the value λ as $t \rightarrow \infty$ describe the nature of the intermittency.

Another way of characterising the temporal intermittency, essentially equivalent to the analysis of the distribution of finite-time decay rates, considers the decay of ensemble-averaged moments of the scalar concentration, that is, of ensemble averages of various powers p of the concentration. This is a standard approach for finite-dimensional dynamical systems [6–8] where these moment decay rates, which we denote by γ_p , are termed ‘generalised Lyapunov exponents’. They turn out to encapsulate the same information as the distribution of finite-time Lyapunov exponents, at least asymptotically for large time. In terms of these moment decay rates, temporal intermittency is revealed by a nonlinear dependence of γ_p on p . A strong intermittency then implies that the γ_p cannot be inferred from infinite-time decay rate λ or, conversely, that λ cannot be inferred from knowledge of a particular γ_p . The latter point is the most relevant in practice: it is often easier to develop a theory predicting the decay rate of some moment, usually the variance ($p = 2$), and indeed, theories of this

type have been developed for some classes of flows, notably chaotic, mixing flows [9–14] and flows with no-slip boundary conditions [15, 16]. The genuine need, however, is for predictions that are relevant to single flow realisations, specifically for the decay rate λ and, if possible, for some information about the distribution of finite-time decay rates λ_t . Whether such predictions can be reliably inferred from variance or other moment decay rates depends on how intermittent the scalar decay is, with a strong intermittency making this type of inference impossible.

Although the issue of temporal intermittency for decaying scalar has been raised earlier [12, 17], it does not appear to have been analysed in the strange-eigenmode regime that characterises the long-time decay in bounded domains. The aim of the present paper is to carry out such an analysis for two model flows, namely two simple unidirectional shear flows, with periodic spatial dependence and random time dependence. Random shear flows have been studied a great deal [18–21]. The main aim of these studies is the explicit demonstration of the *spatial* intermittency of the decaying scalar — essentially the non-Gaussian nature of the distribution of concentration values at fixed time — and the flow that they examine typically is a linear shear in an unbounded domain. A notable exception is the work by Bronski and McLaughlin [22] who examined scalar decay in a sinusoidal shear flow, in particular with periodic boundary conditions for the scalar concentration. We reconsider this flow or, rather, a slight extension thereof with finite rather than vanishing correlation time. Specifically, we study advection–diffusion in a velocity field of the form $(u, v) = (0, V(x, t))$, with

$$V(x, t) = f(t) \sin x \tag{1.1}$$

for a stationary random function $f(t)$ which we take to be piecewise constant. Periodic boundary conditions are imposed for the scalar concentration in both the x - and y -directions, thus ensuring strange-eigenmode decay in the long-time limit. As will become apparent, a crucial feature of (1.1) is that only the amplitude is random: the spatial structure is fixed. Our interest is for the decay in the regime where advection dominates diffusion, at least at the flow scale; this is the large-Péclet-number regime thought to be relevant to many applications. In this regime, because the scalar decay is slow compared with the correlation time of $f(t)$, the latter can be formally taken to vanish, and the Bronski and McLaughlin

[22] model is recovered.

In unidirectional flows such as (1.1), the decay of the scalar is accelerated by the shearing effect compared with decay by diffusion alone. This acceleration is however limited by the presence of shearless points, the extrema $x = \pi/2$ and $x = 3\pi/2$ of the velocity profile. This has been noted for time-independent flows ($f(t) = \text{const.}$) by a number of authors [23–25] who found that the concentration decreases to zero very rapidly outside narrow regions around the velocity extrema. The width of these regions then scales with the diffusivity κ like $\kappa^{1/4}$, leading to a decay rate proportional to $\kappa^{1/2}$. Because time-independent flows provide a reference with which to compare random flows, we present in Appendix A.1 a boundary-layer solution of the eigenvalue problem which yields the $\kappa^{1/2}$ dependence of the decay rate when $f(t) = \text{const.}$ We perform a similar boundary-layer analysis for (1.1) with time-dependent random $f(t)$ and, after scaling, reduce the advection–diffusion equation to a pair of coupled stochastic differential equations independent of diffusivity. The behaviour of the scalar decay, including the temporal intermittency, is completely described by these equations. We conclude, in particular, that the decay rate λ and the moment decay rates γ_p all scale like $\kappa^{2/3}$. The intermittency of the decay, although non-zero, turns out to be weak, so that inferring λ from γ_2 , say, leads to an error of only a few percent.

A much stronger intermittency is found for the second type of flow that we examine, with velocity

$$V(x, t) = \alpha \sin(x + \phi(t)), \quad (1.2)$$

where α is a constant and $\phi(t)$ is a stationary random function, uniformly distributed in $[0, 2\pi]$. In contrast with (1.1), this flow has a changing spatial structure, in fact, a randomly translating spatial structure. This makes the scalar evolution much more complicated: as with (1.1), the concentration is localised in the vicinity of two points, but these move randomly in time and do not coincide with the extrema of (1.2). In other words, the decaying process leads to the formation of randomly translating structures in the scalar field which are not phase locked with the advecting velocity field. We document this phenomenon by presenting detailed results of numerical simulations. These reveal a strong intermittency which increases as diffusivity decreases. The intermittency becomes in fact arbitrarily large

as $\kappa \rightarrow 0$, with the moment decay rates γ_p scaling like $\kappa^{1/2}$ while the decay rate λ scales like $\kappa^{3/8}$. Thus, for the flow (1.2) even the power-law dependence of the decay rate in each realisation cannot be inferred from the decay rates of ensemble-averaged quantities. It should however be emphasised that the strange-eigenmode phase of the scalar decay sets in after an asymptotically long transient period; by the end of this period the concentration has decayed to an asymptotically small fraction of its initial value.

The remainder of this paper is structured as follows. In section 2, we introduce our notation for the advection–diffusion problem and define the various decay rates (finite-time, infinite-time and of ensemble-averaged moments) used to diagnose temporal intermittency. We examine the scalar evolution in the velocity fields (1.1) and (1.2) in sections 3 and 4, respectively. The paper concludes with a Discussion in section 5. Some technical details, in particular the boundary-layer analyses leading to the variance decay rates, are relegated to Appendices.

2 Scalar decay in random shear flows

The concentration $C(x, y, t)$ of a passive scalar advected by a shear flow $(u, v) = (0, V(x, t))$ in two dimensions obeys the advection–diffusion equation

$$C_t + V(x, t)C_y = \kappa(C_{xx} + C_{yy}), \quad (2.1)$$

where κ is the diffusivity. Because we consider the effect of varying κ , and in particular taking the limit $\kappa \rightarrow 0$, while keeping $V(x, t)$ fixed, κ can be thought of as the inverse of the Péclet number.

For periodic boundary conditions in the y -direction, as assumed here, $C(x, y, t)$ is the sum of independently evolving Fourier components. We consider one such component and write the concentration as

$$C(x, y, t) = \text{Re} \left[e^{ily - \kappa l^2 t} \hat{C}(x, t) \right],$$

where l is one of the wavenumbers $2n\pi/L$ for $n = \pm 1, \pm 2, \dots$, and L is the domain period in the y -direction. The complex amplitude $\hat{C}(x, t)$ then satisfies

$$\hat{C}_t + ilV(x, t)\hat{C} = \kappa\hat{C}_{xx}. \quad (2.2)$$

Note that we do not consider the y -independent ($l = 0$) component which is unaffected by the flow and hence decays purely diffusively.

We focus on the decay of the concentration when $V(x, t)$ is a random function of time with smooth spatial structure, and we assume that $V(x, t)$ and $\hat{C}(x, t)$ are 2π -periodic in x . This decay is expected to be exponential in the long time limit; specifically, the ergodic multiplicative theory [3, 4] applied to the advection–diffusion equation suggests that

$$\hat{C}(x, t) \sim D(x, t) \exp(-\lambda t) \quad \text{as } t \rightarrow \infty, \quad (2.3)$$

for almost all realisations of $V(x, t)$.¹ Here, $\lambda > 0$ is the decay rate and is deterministic, and $D(x, t)$ is a (complex) stationary random function describing what Pierrehumbert [1] termed the strange eigenmode. λ is best thought of as (the negative of) the Lyapunov exponent of (2.2), defined by

$$\lambda = - \lim_{t \rightarrow \infty} \frac{1}{t} \log \frac{\|\hat{C}\|(t)}{\|\hat{C}\|(0)}, \quad (2.4)$$

where we use the usual L_2 norm

$$\|\hat{C}\|(t) = \left[\int |\hat{C}(x, t)|^2 dx \right]^{1/2}.$$

Because it is deterministic, λ characterises the decay of almost all realisations of the flow and provides the most useful measure of the mixing efficiency for large times.

The temporal intermittency of the scalar decay can be quantified by considering the finite-time decay rates, or finite-time Lyapunov exponents, defined by

$$\lambda_t = -\frac{1}{t} \log \frac{\|\hat{C}\|(t)}{\|\hat{C}\|(0)}, \quad (2.5)$$

and the moment decay rates γ_p , defined by

$$\gamma_p = - \lim_{t \rightarrow \infty} \frac{1}{t} \log \frac{\mathbf{E} \|\hat{C}\|^p(t)}{\|\hat{C}\|^p(0)}, \quad (2.6)$$

¹We remain at a heuristic level and do not provide here a rigorous justification for the applicability of the ergodic multiplicative theory to the advection–diffusion equation. This would require either an infinite-dimensional version of this theory [26] or reduction to a finite-dimensional problem using inertial-manifold arguments [27]. Furthermore, statements such as (2.3) would need to be made precise using both forward and backward evolution [3].

where \mathbf{E} denotes the mathematical expectation and we take a deterministic initial condition. Note that, because of the form of (2.3), the particular norm chosen for the definitions (2.4) and (2.6) is irrelevant. Thus, $\|\hat{C}\|^p$ could be replaced in (2.6) by

$$\int |\hat{C}(x, t)|^p dx. \quad (2.7)$$

What is crucial, however, is that γ_p characterises the decay of ensemble-averaged moments.

The relationship

$$\lambda = \left. \frac{d\gamma_p}{dp} \right|_{p=0}, \quad (2.8)$$

is readily established from (2.4) and (2.6). The connection between the finite-time distribution of λ_t and the function γ_p for $p \in \mathbb{R}$, which are well-known for finite-dimensional linear systems [5, 6], are expected to also hold for the advection–diffusion equation (2.2). Specifically, if we assume that the probability density function for λ_t takes the large-deviation form

$$p(\lambda_t; t) \sim \left(\frac{g''(\lambda)}{2\pi} \right)^{1/2} e^{-tg(\lambda_t)}, \quad \text{as } t \rightarrow \infty, \quad (2.9)$$

with $g(\cdot)$ a convex, non-negative (Cramer) function satisfying $g(\lambda) = 0$, then it is easy to show using Laplace’s method that the Legendre-transform formula

$$\gamma_p = \inf_{\lambda_t} [p\lambda_t + g(\lambda_t)]. \quad (2.10)$$

holds.

We emphasise that although $\lambda_t \rightarrow \lambda$ as $t \rightarrow \infty$ the non-trivial distribution (2.9) of λ_t for finite t implies that $\gamma_p \neq p\lambda$ in general. Thus, the decay rate γ_p of ensemble-averaged moments $\mathbf{E} \|\hat{C}\|^p$ differs from the decay rate $p\lambda$ of $\|\hat{C}\|^p$ in almost all flow realisations. This reflects the intermittency of the passive-scalar decay which is the focus of the present paper. This intermittency means, in particular, that the decay rate derived for a particular moment, often $p = 2$, cannot be used to infer the decay rate in typical realisations, which is λ . In the next two sections, we examine two types of flows for which the intermittency can be clearly demonstrated by asymptotic and numerical means.

3 Flow with fixed spatial structure

3.1 Model

For the first type of flow, we take the velocity field

$$V(x, t) = f(t) \sin x, \quad (3.1)$$

where $f(t)$ is a zero-mean random function of time. It is then convenient to take the piecewise-constant function

$$f(t) = \alpha \xi_n / l \quad \text{for } n \leq t < n + 1, \quad n = 0, 1, 2, \dots,$$

where $\alpha > 0$ is a constant, the ξ_n are independent normal variables with zero mean and unit variance, and the division by l is introduced for ease of notation. This type of flow is in the class of renewing (or renovating [28]) flows, that is, flows which decorrelate completely in a finite time, taken here to be 1. In such flows, the concentration at the end of each time interval, that is, $\hat{C}_n(x) = \hat{C}(x, n)$ evolves according to a random map. In the absence of diffusion, this map reads

$$\hat{C}(x) \mapsto \hat{C}(x) e^{-i\alpha \xi \sin x}. \quad (3.2)$$

With diffusion, the map is more complicated to write down. A standard simplification is to consider that advection and diffusion act successively: thus, a period of advection leading to the map (3.2) is followed by a period diffusion leading to the map

$$\hat{C}(x) \mapsto e^{\kappa \partial_{xx}^2} \hat{C}(x), \quad (3.3)$$

where $\exp(\kappa \partial_{xx}^2)$ denotes the time-1 flow of the heat equation. Combining (3.2)–(3.3), we write the dynamics as

$$\hat{C}_{n+1}(x) = e^{\kappa \partial_{xx}^2} \left(e^{-i\alpha \xi \sin x} \hat{C}_n(x) \right). \quad (3.4)$$

This is the model that we use for numerical simulations. These are carried out using a pseudo-spectral representation of $\hat{C}_n(x)$, with the advection step (3.2) carried out on the grid, and the diffusion step (3.3) carried out in Fourier space. Following Pierrehumbert [29], we formulate the dynamics on a lattice by constraining the advection to take place over an

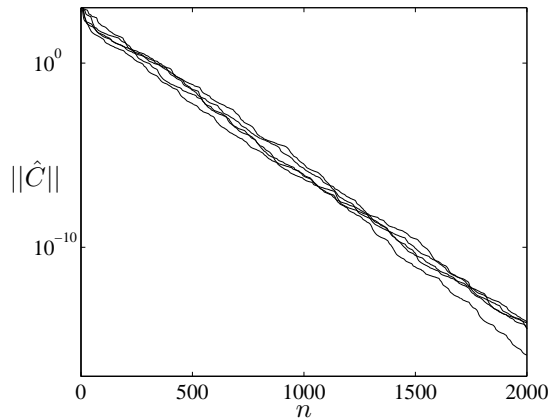


Figure 1: Concentration decay for the advection–diffusion map (3.4) with $\alpha = \pi$ and $\kappa = 10^{-3}$. The norm of the concentration is shown in logarithmic coordinate as a function of the iteration number n for 5 different realisations of the map.

integral number of grid steps. Depending on diffusivity, we use between 512 and 2048 grid points and Fourier modes; this proves sufficient for the results to be insensitive to resolution.

Figure 1 shows the decays of the norm of the concentration in 5 typical realisations of the map (3.4), all taken with the same initial condition $\hat{C}_0 = 1$. As expected, the concentration decays exponentially, with finite-time decay rates λ_n changing from realisation to realisation. This of course is a finite-time effect, and if the simulations were carried out for a larger number of iterations, all the decay rates would converge to the same rate λ . Figure 2 illustrates the spatial structure of the decaying concentration: it shows \hat{C} normalised by $||\hat{C}||$ as a function of x , here after $n = 2000$ iterations of the map. A similar structure is in fact observed at all n after a brief transient period. The modulus of \hat{C} has two well-defined peaks centred at $x = \pi/2$ and $x = 3\pi/2$ and decreases sharply away from these. The real and imaginary parts of \hat{C} oscillate over a scale that is roughly that of the peaks. The width of the peaks changes with n in a random fashion, as does the phase of the oscillations. Numerical experiments with different values of κ show that the decay rate λ and the typical width of the peaks in $|\hat{C}|$ decrease with κ in a power-law fashion. (Note that the symmetry in the two peaks results from the fact that $\hat{C}_0(\pi/2) = \hat{C}_0(3\pi/2) = 1$.) We now develop an asymptotic theory that predicts this power-law behaviour and gives a characterisation of the intermittency of

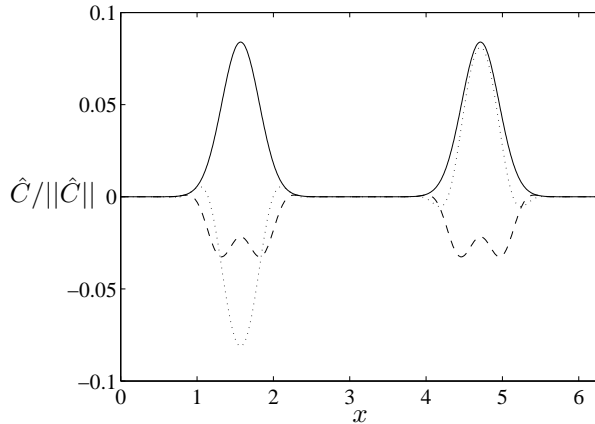


Figure 2: Normalised concentration of the decaying scalar for the advection–diffusion map (3.4). $|\hat{C}|$ (solid line), $\text{Re } \hat{C}$ (dashed line) and $\text{Im } \hat{C}$ (dotted line) normalised by $\|\hat{C}\|$ are shown as functions of x after $n = 2000$ iterations with $\kappa = 10^{-3}$.

the scalar decay for $\kappa \rightarrow 0$.

3.2 Asymptotic results

We start by noting that the decay is slow compared with the correlation time of the velocity field, taken to be unity. We can thus approximate the piecewise-constant process $f(t)$ by a white noise, and write the continuous evolution equation

$$\hat{C}_t + i\alpha \sin x \hat{C} \circ \dot{W}_t = \kappa \hat{C}_{xx}, \quad (3.5)$$

where \dot{W}_t is a white noise, and formally $t = n$. Because the white-noise term emerges as limit of a coloured noise, this equation should be interpreted in the sense of Stratonovich [30] indicated by the symbol \circ .

Equation (3.5) is precisely that studied by Bronski and McLaughlin [22], and clearly it is relevant for velocity fields of the form (3.1) with more general $f(t)$ than the one used for our numerical simulations. The analysis that we now present is fairly different from that of Bronski and McLaughlin [22] in that we focus on the small-diffusivity limit $\kappa \rightarrow 0$ and provide an asymptotic model for the single-realisation behaviour of (3.5) whereas they mostly consider ensemble-averaged moments in the opposite limit $\kappa \gg 1$.

The numerical simulations show that the concentration is localised near the points $x = \pi/2$ and $x = 3\pi/2$ where the shear V_x vanishes, as is the case for constant $f(t)$. This suggests using a boundary-layer approach. Focusing on the neighbourhood of $x = \pi/2$, we let

$$\hat{C}(x, t) = e^{-i\alpha W_t} \tilde{C}(X, T),$$

where W_t is the Wiener process,

$$x = \frac{\pi}{2} + \kappa^{1/6} \alpha^{-1/3} X \quad \text{and} \quad t = (\kappa \alpha)^{-2/3} T. \quad (3.6)$$

Introducing these variables into (3.5), expanding the sine and using the scaling property of W_t , we find the parameter-free leading-order equation

$$\tilde{C}_T - \frac{i}{2} X^2 \tilde{C} \circ \dot{W}_T = \tilde{C}_{XX}.$$

A solution with suitable decay for $|X| \rightarrow \infty$ is found as

$$\tilde{C}(X, T) = e^{-[a(T)X^2 + b(T)]}, \quad (3.7)$$

where the complex amplitudes $a(T)$ and $b(T)$ satisfy the stochastic differential equations

$$\dot{a} = -4a^2 - \frac{i}{2} \dot{W}_T \quad \text{and} \quad \dot{b} = 2a. \quad (3.8)$$

This simple system encapsulates the statistical properties of the scalar decay in the flow (3.1). The finite-time decay rates λ_t , in particular, are given up to scaling by $b(T)/T$, with the long-time limit

$$\lambda = (\kappa \alpha)^{2/3} \lim_{T \rightarrow \infty} \frac{1}{T} \text{Re } b(T) = 2(\kappa \alpha)^{2/3} \text{Re } \mathbb{E} a(T). \quad (3.9)$$

Note the $\kappa^{2/3}$ -scaling, which shows that the scalar decay is much slower in the flow (3.1) with random $f(t)$ than with constant $f(t)$ (in which the decay rate scales like $\kappa^{1/2}$, see Appendix A.1).

Numerical solutions of (3.8) show that $a(T)$ and $b(T)/T$ quickly reach stationary distributions, with $\text{Re } a > 0$ as is required for the localisation of the solution (3.7) assumed for the asymptotics. The form of the solution (3.7) is then consistent with the expected strange-eigenmode decay (2.3), with an eigenmode structure

$$D(x, t) = e^{-i\alpha W_t - a(T)X^2}$$

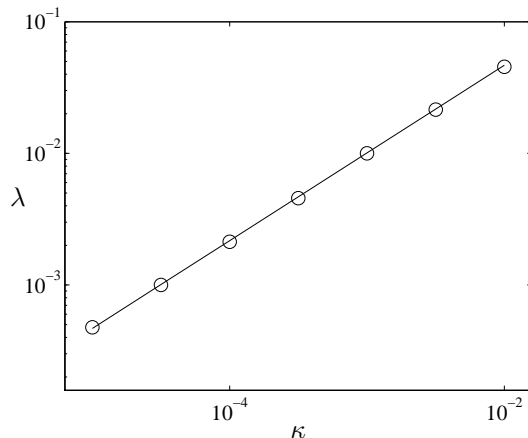


Figure 3: Decay rate λ as a function of diffusivity κ for the advection–diffusion map (3.4) with $\alpha = \pi$. Numerical results (o) are compared with the theoretical prediction (3.10) scaling like $\kappa^{2/3}$ (solid line).

that is indeed stationary. It is also consistent with the form of \hat{C} obtained in numerical experiments with the map (3.4) and illustrated by Figure 2.

We estimate numerically from (3.8) that $2\text{Re } \mathbb{E} a(T) \approx 0.460$, hence we predict the decay rate to be

$$\lambda \sim 0.460(\kappa\alpha)^{2/3}. \quad (3.10)$$

Figure 3 compares this prediction with the decay rate found in numerical simulations of (3.4) for a range of values of κ . To obtain a reliable approximation from such simulations, it is best to run an ensemble of computations and estimate λ as the average of the finite- n decay rate λ_n for large n . A relatively small ensemble, of about 100 realisations, is enough to obtain a reliable estimate for $\mathbb{E} \lambda_n$, which converges to some λ for large n . The results confirm the validity of the theoretical approximation (3.10), with a good agreement even for κ moderately small. In fact, for all the values of κ shown in Figure 3, the relative difference between the approximation (3.10) and the numerical estimate does not exceed 3%.

The moment decay rates γ_p defined in (2.6) can also be inferred from the form (3.7) of the solution as

$$\gamma_p = - \lim_{T \rightarrow \infty} \frac{(\alpha\kappa)^{2/3}}{T} \log \mathbb{E} |e^{-pb(T)}|.$$

This can be estimated by solving (3.8) numerically, although a large ensemble is required for reliable results. Our best estimate for the (ensemble-averaged) variance decay rate, for instance, is

$$\gamma_2 \approx 0.881(\kappa\alpha)^{2/3}. \quad (3.11)$$

This value has been confirmed in two ways. First, we have solved the eigenvalue problem for the covariance $\mathbf{E} \hat{C}^*(x, t) \hat{C}(x', t)$ by a combination of asymptotic and numerical means, as is detailed in Appendix A.2. This reproduces formula (3.11), with an identical numerical factor up to the third significant digit. The second confirmation is obtained by direct ensemble simulations of (3.4). In this manner we obtain, for instance, $\gamma_2 = 0.0886$ for $\kappa = 10^{-2}$ and $\alpha = \pi$ when (3.11) predicts 0.0877.

The results (3.10) and (3.11) show explicitly that the passive-scalar decay is intermittent: $\gamma_2 \neq 2\lambda$, and more generally, $\gamma_p \neq p\lambda$ and $\gamma_p \neq p\gamma_2/2$, as we have verified for $p = 4$ (results not shown). The intermittency turns out to be rather weak, however, with a relative error $|\gamma_2 - 2\lambda|/\gamma_2$ of about 4%; it may well be insignificant for most applications. We emphasise that this weakness is nothing more than a numerical property of the stochastic differential system (3.8): the intermittency cannot be said to be small in any asymptotic sense. In the next section, we consider a different class of shear flows leading to a radically different behaviour for the passive scalar problem, with an intermittency that is asymptotically large as $\kappa \rightarrow 0$.

4 Flow with translating spatial structure

4.1 Model

The type of flow that we now consider has a velocity field of the form

$$V(x, t) = \alpha \sin(x + \phi(t))/l, \quad (4.1)$$

where $\phi(t)$ is a stationary random function of time, distributed uniformly in $[0, 2\pi]$. As before, α is a constant, and the division by the wavenumber l is introduced for ease of notation. Following section 3, we take $\phi(t)$ to be constant for $t \in [n, n + 1)$, with independent values

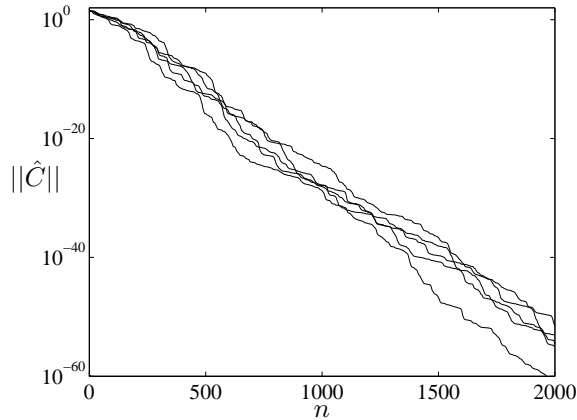


Figure 4: Concentration decay for the advection–diffusion map (4.2) with $\alpha = \pi$ and $\kappa = 10^{-3}$. The norm of the concentration is shown in logarithmic coordinate as a function of the iteration number n for 5 different realisations of the map.

ϕ_n in each interval, and reduce the evolution to a random map. Alternating advection and diffusion steps, we obtain the random map

$$\hat{C}_{n+1}(x) = e^{\kappa \partial_{yy}^2} \left[e^{-i\alpha \sin(x+\phi_n)} \hat{C}_n(x) \right], \quad (4.2)$$

whose dynamics we now examine.

We have carried out a number of numerical experiments with the map (4.2) for a range of values of κ , using an implementation similar to that described in section 3.1. Figure 4 shows the decay of $\|\hat{C}\|$ in five typical realisations of the map for $\kappa = 10^{-3}$ and $\alpha = \pi$ and $\hat{C}_0(x) = 1$. There are two striking features when compared with the decay obtained with the map (3.4) and illustrated in Figure 1: the decay occurs at a much larger rate, and it is much more intermittent. At this point, the intermittency is detected qualitatively in the existence of clear time intervals during which the decay rate is much larger or much smaller than its long-time average. Below, we make more quantitative statements by considering the difference between λ and γ_p/p .

The evolution of the normalised concentration $\hat{C}/\|\hat{C}\|$ is remarkable and deserves to be described in some detail. As in the case of flows with fixed spatial structure, the modulus of the concentration has two well-defined peaks separated by a distance π ; what is different,

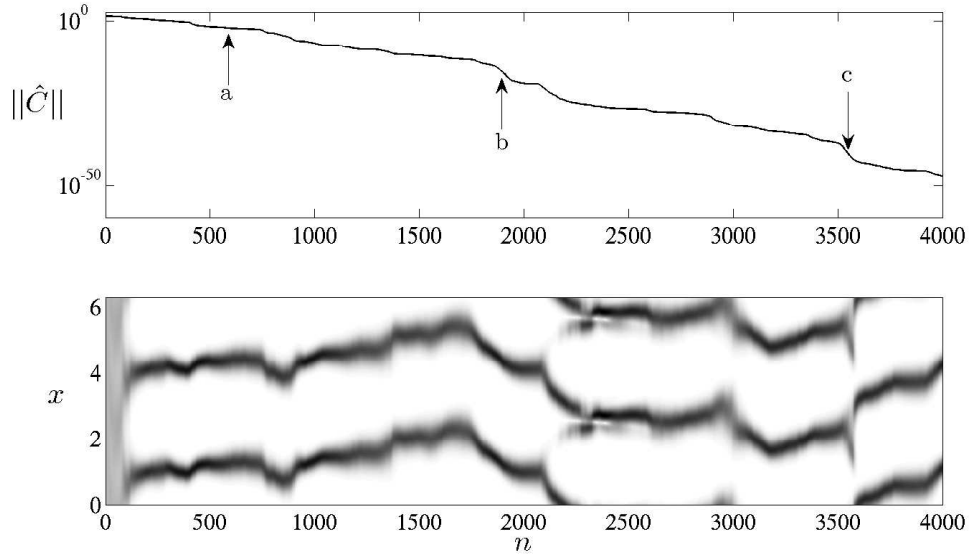


Figure 5: Concentration decay for the advection–diffusion map (4.2) with $\alpha = \pi$ and $\kappa = 10^{-4}$. The top panel shows the norm of the concentration as a function of the iteration number n in one realisation of the map. The bottom panel shows the modulus of the normalised concentration $|\hat{C}|/||\hat{C}||$ in grey scale as a function of n and x . It exemplifies the random motion experienced by the concentration peaks. Three particular iterates, labelled a, b and c are identified; the corresponding concentration profiles are shown in Figure 6.

besides the different scaling with κ of the peak width, is the fact that the peaks are moving over long time scales in a random manner. In addition, the real and imaginary parts of \hat{C} oscillate within the peaks, with a wavelength that changes in time but is typically much shorter than the peak width. To illustrate the nature of evolution further, we show details of one particular realisation with $\kappa = 10^{-4}$ and $\alpha = \pi$ in Figures 5–6. The top panel of Figure 5 shows the variance decay, whilst the bottom panel show the corresponding evolution of $|\hat{C}|/||\hat{C}||$. The random motion of the position of the concentration peaks is clearly seen, as are significant fluctuations in the width of the concentration peaks. It is also noticeable that rapid motion of the concentration peaks, as for instance for $1700 \lesssim n \lesssim 2000$, is associated with anomalously fast variance decay. In addition, one can identify periods during which there are more than two peaks ($n \approx 2300$), or the peaks cease to be well defined ($n \approx 3600$).

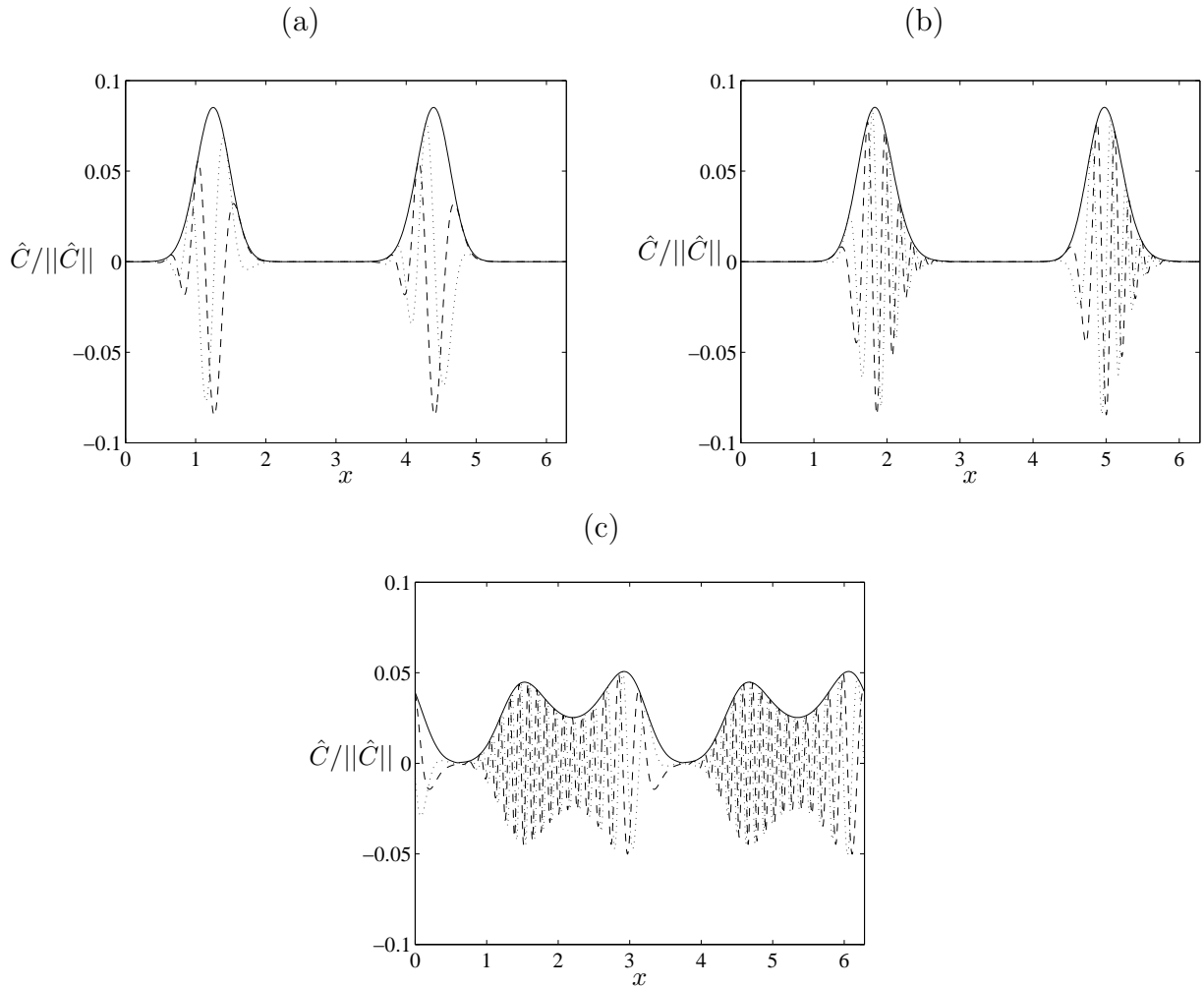


Figure 6: Normalised concentration of the decaying scalar for the realisation of the map (4.2) described in Figure 5. $|\hat{C}|$ (solid line), $\text{Re } \hat{C}$ (dashed line) and $\text{Im } \hat{C}$ (dotted line) normalised by $\|\hat{C}\|$ are shown as functions of x for three iteration numbers $n = 600$ (a), 1780 (b) and 3575 (c) corresponding to the labels in Figure 5. (Enhanced online.)

Following the evolution more closely, e.g. by examining an animation of $|\hat{C}|/\|\hat{C}\|$, shows that these periods, which one might term ‘crises’, correspond to a rapid reorganisation of the concentration structure.

More details of the relationship between the scalar decay and the structure of \hat{C} can be gleaned from Figure 6. This shows the profiles of normalised concentration $|\hat{C}|/\|\hat{C}\|$ for three different values of n identified on Figure 5, namely (a) 600, (b) 1780 and (c) 3575, and

chosen to represent different phases in the evolution. For $n = 600$, the fluctuations in \hat{C} have a moderate scale, shorter than the peak width, but somewhat longer than what an average scale would be. As a result of this moderate scale, the diffusive damping of the concentration is slower than average, and there is little motion of the concentration peaks. For $n = 1780$, by contrast, the scale of fluctuation is very small; as a consequence, the concentration decays sharply. Also, because the smallest scales are on the right of each peak, the dissipation is more intense there, and the peaks move to the left, that is, toward smaller values of x , as can be seen in Figure 5. The iterate $n = 3557$ illustrates the passage through a crisis, when a pair of peaks is being replaced by another, in this case shifted to the right. Again, this can be explained by the changing scale of the oscillations, which favours one pair of peaks by dissipating it less strongly than the other. (Figure 6 is enhanced online by an [animation](#) displaying $\hat{C}/\|\hat{C}\|$ as a function of x for $0 \leq n \leq 4000$ along with $\|\hat{C}\|$ as a function of n .) As the diffusivity κ decreases, the width of the concentration peaks decreases as does the scale of the oscillations within each peak. The decay rate of the concentration and the speed at which the peaks move and change their width also decreases with κ . We quantify this more precisely in the next section.

4.2 Asymptotic results

As in section 3.2, we first point out that the random process in (4.1) can be approximated using white noises in the limit $\kappa \rightarrow 0$. Writing $\sin(x+\phi(t)) = \sin x \cos \phi(t) + \cos x \sin \phi(t)$, and noting that $\cos \phi(t)$ and $\sin \phi(t)$ have zero mean, variance 1/2 and vanishing covariance, we approximate $\sin(x+\phi(t))$ in (4.1) by $\dot{W}_t^1 \sin x + \dot{W}_t^2 \cos x$, where W_t^1 and W_t^2 are independent Wiener processes. Thus, rather than the map (4.2), we can study the evolution equation

$$\hat{C}_t + \frac{i\alpha}{\sqrt{2}} \hat{C} \circ \left(\dot{W}_t^1 \sin x + \dot{W}_t^2 \cos x \right) = \kappa \hat{C}_{xx}. \quad (4.3)$$

This is the analogue for the flow with translating spatial structure of equation (3.5) obtained for the flow with fixed structure. Although the equations are similar, the passive-scalar decay is qualitatively very different in both cases.

Perhaps unsurprisingly given the complicated nature of the dynamics described in the previous section, we found (4.3) much less amenable to an asymptotic treatment than (3.5):

we were not able to reduce the dynamics to a few stochastic differential equations, and we therefore rely on numerical computations to elucidate the dependence of the average decay rate λ on κ . Analytical progress is however possible for the moment decay rates γ_p . We start by decomposing \hat{C} into amplitude and phase according to

$$\hat{C}(x, t) = \rho(x, t)e^{i\theta(x, t)},$$

and derive the following two evolution equations for ρ and θ from (4.3):

$$\rho_t = \kappa\rho_{xx} - \kappa\rho\theta_x^2, \quad (4.4)$$

$$\theta_t = -\frac{\alpha}{\sqrt{2}} \left(\dot{W}_t^1 \sin x + \dot{W}_t^2 \cos x \right) + \kappa \left(\theta_{xx} + 2\frac{\rho_x\theta_x}{\rho} \right). \quad (4.5)$$

For $t = O(1)$, diffusion can be neglected, and the phase is simply given by

$$\theta(x, t) = -\frac{\alpha}{\sqrt{2}} \left(W_t^1 \sin x + W_t^2 \cos x \right), \quad (4.6)$$

where we assume that $\theta(x, 0) = 0$. Thus θ typically grows like $t^{1/2}$. Diffusion first affects the evolution of ρ ; introducing (4.6) into (4.4) and integrating gives the approximation

$$\rho(x, t) \approx \rho_0(x) \exp \left[-\frac{\alpha^2\kappa}{2} \int_0^t \left(W_s^1 \sin x + W_s^2 \cos x \right)^2 ds \right], \quad (4.7)$$

where $\rho_0(x)$ is the initial condition. This expression describes the early stages of the evolution and, in particular, the manner in which two concentration peaks appear near the minima of the argument of the exponential. These minima move, of course, randomly in time.

The approximation (4.7) does not describe the strange-eigenmode stage of the passive-scalar decay, since it predicts a typical decay that is not exponential in time but rather behaving like $\exp(-t^2)$. It is, however, an approximation valid for an asymptotically long time in the limit $\kappa \rightarrow 0$: according to (4.7), it is only for $t = O(\kappa^{-1/2})$ that the gradients of ρ become $O(1)$, and hence it is only for asymptotically longer times that these gradients become significant in (4.4)–(4.5). Figure 7 illustrates this point by comparing the evolution of $\|\hat{C}\|$ in a realisation of the map (4.2) (again for $\kappa = 10^{-4}$ and $\alpha = \pi$) with the prediction deduced from (4.7). There is a good match for n up to about 600; thereafter, the superexponential behaviour that (4.7) entails becomes clear, and the predicted decay becomes much faster than the actual one. We emphasise that the concentration norm has already been reduced

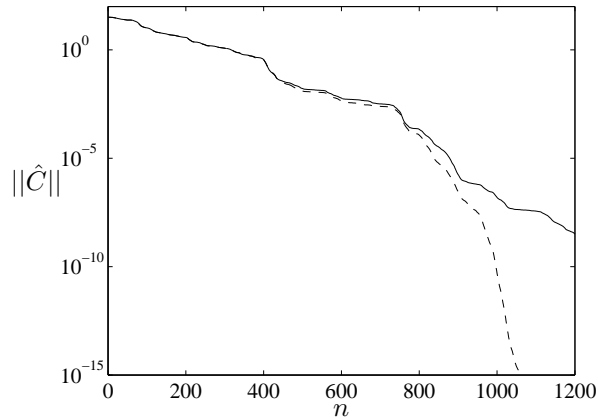


Figure 7: Norm of the concentration $\|\hat{C}\|$ as a function of the iteration number n in one realisation of the random map (4.2) with $\kappa = 10^{-4}$ and $\alpha = \pi$: the numerical result for the map (solid line) is compared with the norm obtained from the asymptotic result (4.7) (dashed line), which holds only for a finite time.

by several orders of magnitudes when (4.7) ceases to be accurate. This is consistent with our remark that (4.7) holds for times longer than $O(\kappa^{-1/2})$, that is, here $n \gg 100$. From a practical viewpoint, then, (4.7) is valuable, since one may not be interested in the evolution of the scalar once its concentration has been reduced to a small fraction of its initial value.

An important feature of (4.7) is that leads to an exponential decay for the moments of ρ and hence of $\|\hat{C}\|$. Indeed, in Appendix B we show that (4.7) implies that

$$\mathbb{E} \rho^p(x, t) \sim \rho_0^p(x) e^{-\alpha(\kappa p)^{1/2} t/2} \quad (4.8)$$

as $t \rightarrow \infty$. We now argue that this result provides the correct large- t asymptotics for the decay rates of the ensemble-averaged moments of $\|\hat{C}\|$, even though it relies on (4.7) which is a valid approximation only for a finite time. The reason for this is that the ensemble-averaged moments are dominated by realisations of the flow for which the scalar decay has been anomalously weak. Thus, at any time, the ensemble-averaged moments are dominated by realisations for which θ is anomalously small and as a consequence, the gradients of ρ are small; these are circumstances which ensure the validity of (4.7). In other words, even though the approximation (4.7) fails at large time for typical realisations, it is applicable

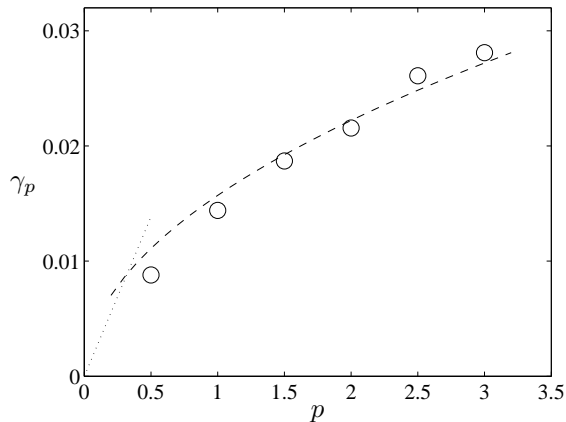


Figure 8: Moment decay rate γ_p as a function of the moment number p for the map (4.2) with $\kappa = 10^{-4}$ and $\alpha = \pi$. Numerical estimates of γ_p (o) are compared with the asymptotic prediction (4.9) valid for $\kappa \ll 1$ (dashed line). The tangent to the curve γ_p at $p = 0$, with slope given by the decay rate λ estimated from (4.10), is also indicated (dotted line).

for those anomalous realisations which dominate the behaviour of the ensemble-averaged moments. As a result, we predict the moment decay rates to be asymptotically

$$\gamma_p \sim \frac{\alpha(\kappa p)^{1/2}}{2} \quad (4.9)$$

as $\kappa \rightarrow 0$. This expression can be confirmed for $p = 2$, that is, for the variance decay rate, by examining the eigenvalue problem for the concentration covariance. This is carried out in Appendix A.3. It proves rather difficult to verify (4.9) through direct numerical simulations. On the one hand prohibitively large ensembles are necessary to obtain estimates of γ_p with $p > 2$; on the other hand, (4.9) is not valid for $p \ll 1$ (see below). Nevertheless, our numerical results, presented in Figure 8 for $\kappa = 10^{-4}$ and $\alpha = \pi$, appear consistent with the estimate (4.9).

The estimate (4.9), with its highly nonlinear $p^{1/2}$ dependence on the moment number p , underlies the strong intermittency of the passive scalar decay for the flow with translating spatial structure. The $p^{1/2}$ has in fact a crucial feature: it is not differentiable at $p = 0$. Hence the relationship (2.8) predicts a infinite decay rate (or Lyapunov) exponent λ . This reflects the fact that the approximation (4.9) is not uniformly valid for $p \rightarrow 0$, and that the

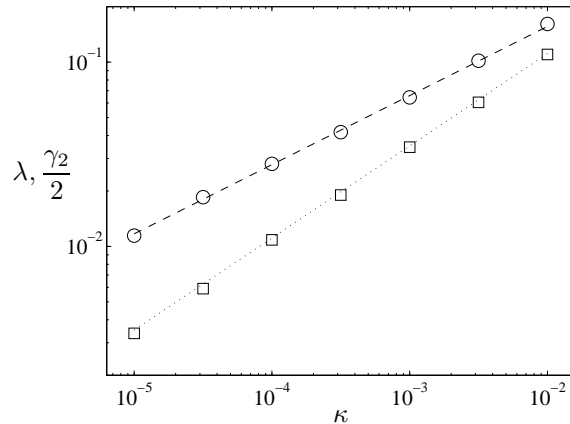


Figure 9: Decay rate λ as a function of diffusivity κ for the map (4.2) with $\alpha = \pi$. Numerical results for λ (\circ) are shown together with the best fit of a $\kappa^{3/8}$ power law (dashed line). Also shown are the numerical results for (half) the decay rate γ_2 of the ensemble-averaged variance (\square), and the $\kappa^{1/2}$ power law predicted by the asymptotic result (4.9) (dotted line). The difference between λ and $\gamma_2/2$ demonstrates that the temporal intermittency of the passive-scalar decay becomes asymptotically large as $\kappa \rightarrow 0$.

dependence of λ upon κ is very different from that of γ_p with $p = O(1)$. Our numerical results establish this clearly: we found that λ depends on κ in a power-law manner with the power appearing to be $3/8$, that is,

$$\lambda \sim a\kappa^{3/8}, \quad (4.10)$$

with a best estimate for the prefactor $a = 0.878$. (The best fit for an arbitrary power law gives $\gamma_p \sim 0.897\kappa^{0.378}$.) Figure 9 illustrates these numerical results by showing λ as a function of κ together with the estimate (4.10) for the map (4.2) with $\alpha = \pi$. The Figure highlights the nature of the intermittency of the passive-scalar decay by also showing $\gamma_2/2$ which clearly differs largely from λ .

Once (4.10) is known, it provides the slope of the tangent of the curve γ_p at $p = 0$. For $\kappa = 10^{-4}$, the numerical value obtained for a is consistent with our numerical results for γ_p , as the plot of the tangent in Figure 9 indicates. The $\kappa^{3/8}$ of the slope of γ_p at the origin, and the $(\kappa p)^{1/2}$ dependence of γ_p for $p = O(1)$ suggest that there is a cross-over between

two different regimes for $p = O(\kappa^{1/4})$. The Legendre transform formula (2.10) then implies that the Cramer function governing the distribution of finite-time decay rates λ_t , while some $O(1)$ function for $\lambda = O(\kappa^{3/8})$, is proportional to κ/λ_t for much smaller values of λ_t .

In summary, flows of the type (4.1) prove to be extreme examples of the temporal intermittency that is possible in passive-scalar decay. With the different power-law dependence of λ and γ_p on κ , the intermittency, measured for instance by $|\gamma_2 - 2\lambda|/\gamma_2$, is arbitrary large in the limit $\kappa \rightarrow 0$. We have not been able to develop an asymptotic theory for the system (4.2) which describes the strange eigenmode structure and evolution in a κ -independent manner. Extensive numerical simulations for different values of κ have however led to the identification of some scalings in addition to that of the decay rates (4.9)–(4.10). Specifically, the scale of variation of ρ appears proportional to $\kappa^{1/8}$, with the form $\exp[-b(x - c)^2/\kappa^{1/4}]$, where b and c $O(1)$ functions of time, giving a good match for the structure of ρ in the neighbourhood of its peak values. Also, the evolution of ρ , that is, the change in the values of the parameters b and c just introduced, appears to take place over an $O(\kappa^{-3/4})$ time scale. Together with (4.10) this implies that the concentration has decayed by a factor proportional to $\exp(-d\kappa^{-3/8})$, for some order-one constant d , by the time the strange-eigenmode stage is reached.

5 Discussion

The two random shear flows considered in this paper illustrate the intermittent nature of the decay of a passive scalar advected and diffused in a bounded domain. For the first flow, with fixed spatial structure, the intermittency turns out to be weak, even though not asymptotically small the limit of vanishing diffusivity (large Péclet number). In this case the intermittency can probably be ignored for practical purposes: the decay rate of the ensemble-averaged p -th moment is nearly linear in p , and $\gamma_2/2$ for instance can be used to predict the decay rate λ in individual realisations of the flow. It should be stressed, however, that because the intermittency is of order one in an asymptotic sense and only numerically small, it may well be significant for other flows with fixed spatial structure, for instance given by a superposition of Fourier modes rather than a single mode.

The second type of flow that we consider, with randomly translating spatial structure, displays a spectacular form of intermittency in the limit of small diffusivity. For this flow, the power-law dependence on diffusivity of the decay rate λ differs from that of the moment decay rate γ_p , with respective dependences in $\kappa^{3/8}$ and $\kappa^{1/2}$, respectively. Thus in each individual realisation, the passive scalar concentration decreases at a rate that is much larger than what ensemble-averaged results might suggest. As explained, this is because ensemble averages are dominated by anomalous realisations in which the scalar decay is much slower than is typical. We also note that the time scale necessary for the long-time stage of decay (the strange-eigenmode stage) to be reached is asymptotically long, so that the concentration is reduced to a vanishingly small fraction of its initial value by the time this stage is reached. This may limit the relevance of the strange-eigenmode stage for applications.

Although the paper is mainly focused on the issue of intermittency, it is useful to note what the effect of randomness is on the efficiency of the mixing as measured by the decay rate λ . As Appendix A.1 recalls, the decay rate for a time-independent sinusoidal flow (and more generally for any flow with extrema), is proportional to $\kappa^{1/2}$. Making the amplitude of the sinusoid a zero-mean random function of time as in (3.1) unsurprisingly diminishes the efficiency of the mixing, with a decay rate scaling like $\kappa^{2/3}$. Making the phase of the sinusoid vary randomly in time as in (4.1), by contrast, makes the mixing more effective; this is because the extrema of the velocity profile, which limit mixing when the spatial structure of the flow is fixed, constantly change position so that no regions of the fluid remain unaffected by shear. The result is a decay rate proportional to $\kappa^{3/8}$. In a natural way, this is larger than the $O(\kappa^{1/2})$ decay rate achieved for time-independent flows with extrema, but smaller than the $O(\kappa^{1/3})$ found for monotonic velocity profiles [23, 24]. Of course, the latter cannot be continuous in periodic domains. Note that through a change of reference frame the flow (4.1) can be reinterpreted as the two-dimensional velocity field $(u, v) = (\dot{\phi}, \alpha \sin x/l)$; this has a time-independent shear and a random uniform flow across the shear.

We conclude this paper by returning to the issue of temporal intermittency. Our results show that this intermittency can be significant for a (somewhat contrived) class of shear flows. It is natural to ask whether similar results hold for more general flows and, in particular, for the class of two-dimensional mixing flows in periodic domains which have attracted so much

attention in the last few years [1, 9, 11–14, 29]. Recently, Haynes and Vanneste [12] showed that two distinct regimes of scalar decay are possible in these flows, depending on the scale of the flow relative to the domain size. In the first regime, termed locally controlled, the scalar decay is limited by small regions of the fluid which have experienced anomalously low stretching and hence have relatively high scalar concentration. In the second regime, termed globally controlled, the scalar field has a large-scale structure roughly determined by the gravest mode of the Laplacian in the domain. It is likely that the temporal intermittency properties differ between the two regimes. It can in fact be anticipated to be weak in the locally controlled regime, where some self-averaging is expected to take place because of the smallness of the scalar structures involved. Haynes and Vanneste [12] reported only small differences between the decay rate γ_2 and half the (ensemble-averaged-)variance decay rate $\gamma_2/2$ in both regimes. It would clearly be desirable to assess in more details the nature of the intermittency for these mixing flows, particularly because the practical use of theoretical predictions relies implicitly or explicitly on the assumption that it is negligible.

Acknowledgements. This work stems from discussions with P. H. Haynes. It is a pleasure to acknowledge helpful conversations with E. Vanden Eijnden. J. V. is funded by a NERC Advanced Research Fellowship.

A Three eigenvalue problems

A.1 Constant flow

For reference we derive the decay rate of a passive scalar in the (non-random) constant flow

$$V(x) = \alpha \sin x/l \tag{A.1}$$

in the limit $\kappa \rightarrow 0$. The decay rate is the real part of the eigenvalue λ satisfying

$$-\lambda \hat{C} + i\alpha \sin x \hat{C} = \kappa \hat{C}_{xx},$$

where $\hat{C}(x)$ is the eigenfunction. As discussed in Giona et al. [24], the eigenfunction is localised near the extrema of $V(x)$, here at $x = \pi/2$ and $3\pi/2$. The eigenvalue problem can

therefore be solved using a boundary-layer method. Focusing on the maximum at $x = \pi/2$, we let

$$x = \frac{\pi}{2} + \kappa^{1/4} \alpha^{-1/4} X \quad \text{and} \quad \lambda = i\alpha + (\kappa\alpha)^{1/2} \tilde{\lambda}$$

and find the leading order equation

$$-\tilde{\lambda} \hat{C} = \frac{iX^2}{2} \hat{C} + \hat{C}_{XX}.$$

Introducing a solution of the form $\hat{C} = \exp(-aX^2)$, we find that

$$a = \frac{1}{4} - \frac{i}{4} \quad \text{and} \quad \tilde{\lambda} = \frac{1}{2} - \frac{i}{2}.$$

Thus the decay rate is

$$\text{Re } \lambda = \frac{(\kappa\alpha)^{1/2}}{2}. \quad (\text{A.2})$$

This formula also applies to flows more general than (A.1), with any number of (non-degenerate extrema), in which case $\alpha/|l|$ is the minimum value of $|V''|$ at these extrema.

A.2 Flow with fixed spatial structure

In this Appendix we derive a closed evolution equation for the concentration covariance

$$\Gamma_n(x, x') = \mathbf{E} \hat{C}_n^*(x) \hat{C}_n(x') \quad (\text{A.3})$$

for the map (3.4). We then solve the corresponding eigenvalue problem asymptotically in the limit $\kappa \rightarrow 0$. We also verify that this eigenvalue problem is identical to leading order to the one that emerges from the continuous-time approximation (3.5).

From (3.4), we obtain that the covariance evolves according to the deterministic map

$$\Gamma_{n+1}(x, x') = e^{\kappa(\partial_{xx}^2 + \partial_{x'x'}^2)} \left[e^{-\alpha^2(\sin x - \sin x')^2/2} \Gamma_n(x, x') \right]. \quad (\text{A.4})$$

This can be written in a more explicit form by introducing the Green's function $G(x - y)$ of the heat equation in $[0, 2\pi]$, such that

$$\exp(-\kappa \partial_{xx}^2) h(x) = \int_0^{2\pi} G(x - y) h(y) dy,$$

for any function h . (Note that y is used here as a dummy integration variable; there should be no confusion with its earlier use as streamwise coordinate.) In the limit $\kappa \rightarrow 0$, $G(x - y)$ reduces to the Green's function of the diffusion equation in an infinite domain, that is

$$G(x - y) \sim \frac{e^{-(x-y)^2/(4\kappa)}}{(4\pi\kappa)^{1/2}}. \quad (\text{A.5})$$

The long-time decay of $\Gamma_n(x, x')$ and hence of the ensemble-averaged variance

$$\mathbf{E} \|\hat{C}\|^2 = \int \Gamma_n(x, x) dx$$

is controlled by the solution of the eigenproblem associated with (A.4). Noting that, according to the definition (2.6), the eigenvalue is $\exp(-\gamma_2)$, we write this eigenvalue problem as

$$e^{-\gamma_2} \Gamma(x, x') = \int_0^{2\pi} \int_0^{2\pi} G(x - y) G(x' - y') e^{-\alpha^2(\sin y - \sin y')^2/2} \Gamma(y, y') dy dy'. \quad (\text{A.6})$$

We now examine this eigenvalue problem in the limit $\kappa \rightarrow 0$. We first note that, for $\kappa = 0$, the eigenvalue problem reduces to

$$e^{-\gamma_2} \Gamma(x, x') = e^{-\alpha^2(\sin x - \sin x')^2/2} \Gamma(x, x').$$

Clearly, the spectrum for γ_2 becomes the range of $\alpha^2(\sin x - \sin x')^2$. For $0 < \kappa \ll 1$, we expect the eigenfunctions associated with small γ_2 to be localised near the minimum of $(\sin x - \sin x')^2$, that is, along the lines $x' = x$ and $x' = \pi - x$ (and their periodic copies). The eigenfunction corresponding to the minimum value of γ_2 is localised near the intersection $x = x' = \pi/2$ of these lines. We identify the relevant scale of localisation as $\kappa^{1/6}$ and hence introduce

$$x = \frac{\pi}{2} + \kappa^{1/6} \alpha^{-1/3} X, \quad \gamma_2 = (\kappa \alpha)^{2/3} \tilde{\gamma}_2, \quad (\text{A.7})$$

(cf. (3.6)) with similar definitions for X' , and regard Γ as a function of X and X' . Expanding in Taylor series and using (A.5) in (A.6) then leads to

$$-\tilde{\gamma}_2 \Gamma = \Gamma_{XX} + \Gamma_{X'X'} - \frac{(X^2 - X'^2)^2}{8} \Gamma. \quad (\text{A.8})$$

The boundary conditions completing the formulation of the asymptotic eigenvalue problem are of course decay for $|X|, |X'| \rightarrow \infty$.

Finding the smallest eigenvalue $\tilde{\gamma}_2$ of (A.8) provides the leading-order approximation to the ensemble-averaged variance decay rate. This needs to be done numerically. We have obtained an approximation to $\tilde{\gamma}_2$ and the corresponding eigenfunction by solving the evolution equation associated with (A.8) numerically, using a finite-difference discretisation. Starting from Gaussian initial condition we obtain the approximation $\tilde{\gamma}_2 \approx 0.8806$, consistent with the results of section 3.2 as well as the structure of the eigenfunction $\Gamma(X, X', t)$ (not shown).

For completeness, we now establish that the eigenvalue problem (A.8) also follows from the continuous-time equation (3.5) which approximates the map (3.4) for $\kappa \rightarrow 0$. From (3.5), we find that

$$\begin{aligned} \partial_t \left[\hat{C}^*(x, t) \hat{C}(x', t) \right] &= \kappa \left[\hat{C}_{xx}^*(x, t) \hat{C}(x', t) + \hat{C}^*(x, t) \hat{C}_{x'x'}(x', t) \right] \\ &\quad + i\alpha(\sin x - \sin x') \hat{C}^*(x, t) \hat{C}(x', t) \circ \dot{W}_t. \end{aligned}$$

Upon transforming into the corresponding Ito form and taking the expectation, we obtain the Schrödinger equation [cf. 22]

$$\Gamma_t = \kappa(\Gamma_{xx} + \Gamma_{x'x'}) - \frac{\alpha^2}{2}(\sin x - \sin x')^2 \Gamma.$$

Introducing eigensolutions $\exp(-\gamma_2 t) \Gamma(X, X')$ with the scaled variables (A.7) and expanding as $\kappa \rightarrow 0$, we recover the eigenvalue problem (A.8). We emphasise that this eigenproblem differs from the one that arises in a linear shear, as studied by Majda [18] and McLaughlin and Majda [20].

A.3 Flow with translating spatial structure

We derive and solve asymptotically the eigenvalue problem that governs the covariance (A.3) for the map (4.2). Because (4.2) is spatially homogeneous, the covariance depends only on $x - x'$, and it is therefore best written as

$$\Gamma_n(x) = \mathbf{E} \hat{C}_n^*(x') \hat{C}_n(x' + x).$$

From (4.2) we obtain that this function evolves according to

$$\Gamma_{n+1}(x) = \int_0^{2\pi} \mathcal{G}(x - x') J_0(2\alpha \sin(x'/2)) \Gamma_n(x') dy', \quad (\text{A.9})$$

where

$$\mathcal{G}(x) = \int_0^{2\pi} G(x-x')G(x') dx'$$

$J_0(\cdot)$ is the 0-th Bessel function of the first kind, and $G(x-x')$ is the Green's function of heat equation, as in Appendix A.2. Using (A.5) gives the asymptotic behaviour

$$\mathcal{G}(x) \sim \frac{e^{-x^2/(8\kappa)}}{(8\pi\kappa)^{1/2}} \text{ as } \kappa \rightarrow 0.$$

The large- n decay of Γ_n and hence of the decay rate γ_2 of the variance are determined by the maximum eigenvalue of the operator on the right-hand side of (A.9). Solving this eigenvalue problem asymptotically for $\kappa \rightarrow 0$ gives an approximation to γ_2 . First note that for $\kappa = 0$, the eigenvalue problem becomes

$$e^{-\gamma_2}\Gamma(x) = J_0(2\alpha \sin(x/2))\Gamma(x).$$

The corresponding spectrum for $e^{-\gamma_2}$ (A.9) becomes the range of $J_0(2\alpha \sin(x/2))$, with maximum $\lambda = 1$ and associated quasi-eigenfunction $\Gamma(x) = \delta(x)$. We therefore expect γ_2 for $\kappa \ll 10$ to be near 0, with eigenfunction localised near $y = 0$. We identify the relevant scale for this localisation as $\kappa^{1/4}$. We introduce the rescaled variables X and $\tilde{\gamma}_2$ defined by

$$x = \kappa^{1/4}\alpha^{-1/2}X \quad \text{and} \quad \gamma_2 = \kappa^{1/2}\alpha\tilde{\gamma}_2 \tag{A.10}$$

and approximate the eigenvalue problem as

$$\begin{aligned} (1 - \kappa^{1/2}\alpha\tilde{\gamma}_2 + \dots)\Gamma(X) &= \frac{1}{(8\pi\alpha)^{1/2}\kappa^{1/4}} \int_{-\infty}^{\infty} e^{-(X-X')^2/(8\kappa^{1/2}\alpha)} \\ &\quad \times \left(1 - \frac{\alpha\kappa^{1/2}}{4}X'^2 + \dots\right)\Gamma(X') dX' \\ &= \Gamma(X) - \frac{\kappa^{1/2}\alpha Y^2}{4}\Gamma(X) + 2\kappa^{1/2}\alpha\Gamma''(X) + \dots \end{aligned}$$

To leading order, the covariance $\Gamma(X)$ and decay rate γ_2 thus satisfy the eigenvalue problem,

$$\Gamma'' + \left(\frac{\tilde{\gamma}_2}{2} - \frac{X^2}{8}\right)\Gamma = 0, \tag{A.11}$$

with solutions decaying for $|X| \rightarrow \infty$ provided that $\tilde{\gamma}_2/(\sqrt{2}) = 1/2 + m$, $m = 0, 1, \dots$. This leads to the variance decay rate and associated eigenfunction

$$\gamma_2 = \alpha \left(\frac{\kappa}{2}\right)^{1/2} + o(\kappa^{1/2}) \quad \text{and} \quad \Gamma(x) = \exp\left(-\frac{\alpha x^2}{4(2\kappa)^{1/2}}\right) + o(1),$$

in agreement with (4.9).

We conclude this Appendix by showing that the eigenvalue problem (A.11) also follows from the continuous-time equation (4.3) which we claim approximates (4.2) for $\kappa \rightarrow 0$. From (4.3) we compute

$$\begin{aligned} \partial_t \left[\hat{C}^*(x, t) \hat{C}(x', t) \right] &= \kappa \left[\hat{C}_{xx}^*(x, t) \hat{C}(x', t) + \hat{C}^*(x, t) \hat{C}_{x'x'}(x', t) \right] \\ &\quad + \frac{i\alpha}{\sqrt{2}} \hat{C}^*(x, t) \hat{C}(x', t) \circ \left[\dot{W}_t^1 (\sin x - \sin x') + \dot{W}_t^2 (\cos x - \cos x') \right]. \end{aligned}$$

Transforming into the Ito form, taking the expectation and replacing $x - x'$ by x leads to

$$\Gamma_t = 2\kappa\Gamma_{xx} - \alpha^2 \sin^2(x/2)\Gamma.$$

The associate eigenvalue problem reduces to (A.11) to leading order in κ when the scaling (A.10) is introduced.

B Expectation of ρ^p

In this Appendix, we show that (4.7) implies (4.8). We represent the two Wiener processes W_t^i , $i = 1, 2$ by their Karhunen–Loève expansion [31, 32], which reads

$$W_t^i = \sum_{k=0}^{\infty} \zeta_k^i \lambda_k^{1/2} \phi_k(t), \quad \text{where } \lambda_k = \frac{4}{(2k+1)^2 \pi^2}, \quad \phi_k(t) = \sqrt{2} \sin(\lambda_k^{-1/2} t),$$

and the ζ_k^i are i.i.d. $N(0,1)$ variables. Using the orthogonality of the $\phi_k(t)$ we obtain from (4.7) that [21]

$$\begin{aligned} \mathbb{E} \rho^p(x, t) &= \rho_0^p(x) \mathbb{E} \exp \left[-\frac{\alpha^2 \kappa p t^2}{2} \sum_k \lambda_k (\xi_k^1 \sin x + \xi_k^2 \cos x)^2 \right] \\ &= \rho_0^p(x) \mathbb{E} \prod_k \exp \left[-\frac{\alpha^2 \kappa p t^2}{2} \lambda_k (\xi_k^1 \sin x + \xi_k^2 \cos x)^2 \right] \\ &= \rho_0^p(x) \prod_k \frac{1}{2\pi} \int_{-\infty}^{\infty} \int_{-\infty}^{\infty} e^{-\alpha^2 \kappa p t^2 \lambda_k (\xi^1 \sin x + \xi^2 \cos x)^2 / 2} e^{-[(\xi^1)^2 + (\xi^2)^2] / 2} d\xi^1 d\xi^2 \\ &= \rho_0^p(x) \prod_k \frac{1}{2\pi} \int_0^{\infty} \int_0^{2\pi} e^{-\alpha^2 \kappa p t^2 \lambda_k r^2 \sin^2 \varphi / 2} e^{-r^2 / 2} r dr d\varphi. \end{aligned}$$

To deduce the last equality, we have introduced the polar coordinates (r, φ) defined by

$$\xi^1 = r \cos(\varphi - x) \quad \text{and} \quad \xi^2 = r \sin(\varphi - x).$$

Carrying out the integration with respect to r , then that with respect to φ , we finally find

$$\mathbb{E} \rho^p(x, t) = \rho_0^p(x) \prod_k \frac{1}{(1 + \alpha^2 \kappa p t^2 \lambda_k)} = \frac{\rho_0^p(x)}{\cosh^{1/2} [\alpha (\kappa p)^{1/2} t]}.$$

The approximation (4.8) follows for large t .

References

- [1] R. T. Pierrehumbert. Tracer microstructure in the large-eddy dominated regime. *Chaos, Solitons & Fractals*, 4:1091–1110, 1994.
- [2] J. Sukhatme and R. T. Pierrehumbert. Decay of passive scalars under the action of single scale smooth velocity fields in bounded two-dimensional domains: from non-self-similar probability distribution functions to self-similar eigenmodes. *Phys. Rev. E*, 66: 056302, 2002.
- [3] L. Arnold. *Random dynamical systems*. Springer, 1998.
- [4] V. I. Oseledec. A multiplicative ergodic theorem. Lyapunov characteristic numbers for dynamical systems. *Trans. Moscow Math. Soc.*, 19:197–221, 1968.
- [5] E. Ott. *Chaos in dynamical systems*. Cambridge University Press, 2nd edition, 2002.
- [6] R. Benzi, G. Paladin, G. Parisi, and A. Vulpiani. Characterisation of intermittency in chaotic systems. *J. Phys. A: Math. Gen.*, 18:2157–2165, 1985.
- [7] A. Crisanti, G. Paladin, and A. Vulpiani. Generalized Lyapunov exponents in high-dimensional chaotic dynamics and products of large random matrices. *J. Stat. Phys.*, 53:583–601, 1988.
- [8] G. Paladin, L. Peletti, and A. Vulpiani. Intermittency as multifractality in history space. *J. Phys. A: Math. Gen.*, 19:L991–L996, 1986.
- [9] T. M. Antonsen, Z. Fan, E. Ott, and E. Garcia-Lopez. The role of chaotic orbits in the determination of power spectra of passive scalar. *Phys. Fluids*, 8:3094–3104, 1996.

- [10] E. Balkovsky and A. Fouxon. Universal long-time properties of Lagrangian statistics in the Batchelor regime and their application to the passive scalar problem. *Phys. Rev. E*, 60:4164–4174, 1999.
- [11] D. R. Fereday and P. H. Haynes. Scalar decay in two-dimensional chaotic advection and Batchelor-regime turbulence. *Phys. Fluids*, 16:4359–4370, 2004.
- [12] P. H. Haynes and J. Vanneste. What controls the decay rate of passive scalars in smooth random flows? *Phys. Fluids*, 17:097103, 2005.
- [13] A. A. Schekochihin, P. H. Haynes, and S. C. Cowley. Diffusion of passive scalar in a finite-scale random flow. *Phys. Rev. E*, 70:046304, 2004.
- [14] Y.-K. Tsang, T. M. Antonsen, and E. Ott. Exponential decay of chaotically advected passive scalars in the zero diffusivity limit. *Phys. Rev. E*, 71:066313, 2005.
- [15] M. Chertkov and V. Lebedev. Decay of scalar turbulence revisited. *Phys. Rev. Lett.*, 90:034501, 2004.
- [16] V. V. Lebedev and K. S. Turitsyn. Passive scalar evolution in peripheral regions. *Phys. Rev. E*, 69:036301, 2004.
- [17] S. Childress and A. D. Gilbert. *Stretch, twist, fold: the fast dynamo*. Springer, 1995.
- [18] A. J. Majda. The random uniform shear layer: an explicit example of turbulent diffusion with broad tail probability distributions. *Phys. Fluids A*, 5:1963–1970, 1993.
- [19] A. J. Majda and P. R. Kramer. Simplified models for turbulent diffusion: theory, numerical modelling and physical phenomena. *Phys. Rep.*, 314:237–574, 1999.
- [20] R. McLaughlin and A. J. Majda. An explicit example with non-Gaussian probability distribution for nontrivial scalar mean and fluctuation. *Phys. Fluids*, 8:536–547, 1996.
- [21] E. Vanden Eijnden. Non-Gaussian invariant measures for the Majda model of decaying turbulent transport. *Comm. Pure Appl. Math.*, 54:1–22, 2001.

- [22] J. C. Bronski and R. M. McLaughlin. Scalar intermittency and the ground state of Schrödinger equations. *Phys. Fluids*, 9:181–190, 1997.
- [23] K. Bajer, A. P. Bassom, and A. D. Gilbert. Accelerated diffusion in the centre of a vortex. *J. Fluid Mech.*, 437:395–411, 2001.
- [24] M. Giona, S. Cerbelli, and V. Vitacolonna. Universality and imaginary potentials in advection–diffusion in closed flows. *J. Fluid Mech.*, 513:221–237, 2004.
- [25] J. P. Gleeson, O. M. Roche, J. West, and A. Gelb. Modelling angular micromixers. *SIAM J. Appl. Math.*, 64:1294–1310, 2004.
- [26] D. Ruelle. Characteristic exponents and invariant manifolds in Hilbert space. *Ann. of Math.*, 115:243–290, 1982.
- [27] W. Liu and G. Haller. Strange eigenmodes and decay of variance in the mixing of diffusive tracers. *Physica D*, 188:1–39, 2004.
- [28] Ya. B. Zel’dovich, A. A. Ruzmaikin, S. A. Molchanov, and D. D. Sokolov. Kinematic dynamo problem in a linear velocity field. *J. Fluid Mech.*, 144:1–13, 1984.
- [29] R. T. Pierrehumbert. Lattice models of advection-diffusion. *Chaos*, 10:61–74, 2000.
- [30] C. W. Gardiner. *Handbook of stochastic methods*. Springer–Verlag, 3rd edition, 2004.
- [31] R. J. Adler. *An introduction to continuity, extrema, and related topics for general Gaussian processes*. Institute of Mathematical Statistics, 1990.
- [32] P. E. Kloeden and E. Platen. *Numerical solutions of stochastic differential equations*. Springer, 1992.